

Study of Transient Nuclei near Freezing

Masaharu ISOBE¹ and Berni J. ALDER²

¹*Graduate School of Engineering, Nagoya Institute of Technology, Nagoya, 466-8555, Japan;* ²*Lawrence Livermore National Laboratory, P.O.Box 808, Livermore, CA 94551-9900, USA*

The molasses tail in dense hard core fluids is investigated by extensive event-driven molecular dynamics simulation through the orientational autocorrelation functions. Near the fluid-solid phase transition, there exist three regimes in the relaxation of the pair orientational autocorrelation function, namely the kinetic, molasses (stretched exponential), and diffusional power decay. The density dependence of both the molasses and diffusional power regimes are evaluated and the latter compares with theoretical predictions in three dimensions. The largest cluster at the freezing density of only a few sphere diameter in size persist for only about 30 picoseconds ($\sim 2.8 \times 10^{-11}$ [s]). The most striking observation through the bond orientational order parameter is the dramatic increase of the cluster size as the freezing density is approached.

§1. Introduction

The long slow decaying potential part of the shear-stress autocorrelation function (SACF) has been called the “molasses tail” to differentiate it from the hydrodynamic origin of the long time tail in the velocity autocorrelation function^{1),2)} and to emphasize its relation to the highly viscous glassy state.^{3),4)} The decay of SACFs have been well investigated by mode coupling theory (MCT) and kinetic theory, both leading to the same power form as in the case of the velocity autocorrelation function. This applies to the kinetic part of the shear autocorrelation function, but not to the potential part which is central to the molasses tail. From the numerical point of view, the long time tail of SACF has been computed by several molecular dynamics (MD) simulations in the early 80s; Evans (1980),⁵⁾ Wood & Erpenbeck(1981),⁶⁾ and Morriss & Evans(1985).⁷⁾ These studies seem to show that the long time tail of both the kinetic and potential parts have a power decay consistent with MCT, however, the amplitude of SACF in dense fluids was found to be orders of magnitude greater than predicted. This discrepancy was ascribed to the possibility that the numerical results were not run long enough. However, we show that the tail is caused by slow structural relaxation in the dense liquid around the peak of the structure factor rather than by hydrodynamic phenomena at long wave length. This was the starting point of the theory of glassy transition.^{8),9)} Since then many papers focusing on density fluctuations in the study of the glass transition have been published, however, the microscopic mechanism of the stress field relaxation have not been clarified yet.

Twenty years ago, Ladd and Alder have speculated that the long time tail of the shear stress auto-correlation function near the solid-fluid transition point in the hard sphere system is due to transient crystal nuclei formation.¹⁰⁾ They found that the potential part of the SACF and the angular orientational auto-correlation function (OACF) are identical in the long time limit and show non-algebraic decay in time.

Since the evidence suggested that the reason for non-algebraic decay is structural relaxation rather than hydrodynamic flow, an attempt was made to understand this slow decaying mechanism by decomposing the OACFs into two-, three-, and four-body correlations, however, many of these correlation functions, especially the four-body correlations, have not been obtained accurately due to the computer limitation at that time. Even with today's much better computers, it is not possible to get accurate information on the four body distribution and hence we made an attempt to use what could be learned about the cluster size from the bond orientational parameter. The results, presented here, look promising, and we plan to extend, this nearest neighbour bond order parameter to further neighbours. The prediction of the cooling rate necessary to prevent crystallization requires knowledge of the rate of growth of a cluster the size of a critical solid nucleus and the time it exists in this transient state. Therefore, analysis of this slow decaying process of the OACF and its decomposition into several components is expected to be a key factor in understanding the onset of the glass transition.^{3),4)}

Previously,¹¹⁾ we have reported on a two dimensional system consisting of elastic hard disks at a single density near the solid-fluid transition point placed in a square box with periodic boundary conditions, using a modern fast algorithm based on event-driven MD simulation.¹²⁾ We confirmed the non-algebraic decay (stretched exponential) at intermediate times presumably due to the existence of various sized solid clusters at high densities decaying at different rates. We also determined the length of time for which the biggest such nuclei exists. In this study, we focus on the rapidly increasing time with increasing density for the decay of OACFs and are able to establish the length of time for which the biggest such nuclei exists at each density. We also compare the results to theoretical predictions in the subsequent power law decay. We will further report results for hard spheres for different particle numbers. We use a more efficient program code for calculating pair contributions to the OACFs, allowing for more accurate results.

§2. Decomposition of the Orientational Autocorrelation Function

We focus on the potential part of the SACF $\langle J_{xy}^P(t)J_{xy}^P(0) \rangle$, where J_{xy}^P is the potential part of the momentum current J_{xy}^P , where the molasses tail appears. Since velocities and positions are no longer correlated beyond a few mean collision times, only the orientational part of SACF, namely the OACF $\langle O_{xy}(t)O_{xy}(0) \rangle$ needs to be studied.^{10),11)} $O_{xy}(t)$ is defined as

$$O_{xy}(t) = \sum_c \frac{x_{ij}y_{ij}}{\sigma^2} \delta(t - t_c), \quad (2.1)$$

where \sum_c means contribution at the colliding time t_c at which $(x_{ij}, y_{ij}) = (x_i - x_j, y_i - y_j)$ are the relative positions between hard spheres (disks) i and j .

To avoid the delta function singularity of $O_{xy}(t)$ for hard particles, the alternative Einstein-Helfand expression^{13),14)} involving the second derivative, obtained by the numerical differentiation with five point stencils, is adopted for calculating the correlation function,

$$C(t) = \langle O_{xy}(t)O_{xy}(0) \rangle = \frac{1}{2} \frac{d^2}{dt^2} \langle (G(t) - G(0))^2 \rangle, \quad (2.2)$$

where

$$G(t) = \sum_c \frac{x_{ij}y_{ij}}{\sigma^2} \Theta(t - t_c), \quad (2.3)$$

and where $\Theta(t)$ is the unit step function. There are three independent orientational factors (O_{xy} , O_{yz} , and O_{zx}) in 3D. We introduce the reduced (e.g. Enskog values) orientational function $C^*(s)$ in terms of the reduced time $s = t/t_0$,

$$C^*(s) = \frac{\pi m \sigma^2 t_0}{V \eta_E} C(t), \quad (2.4)$$

where t_0 is the mean free time and η_E is the Enskog shear viscosity. For a hard core fluid, the Enskog shear viscosity can numerically be estimated by the expression of Gass(1971)¹⁵⁾ with the third Sonine polynomial approximation in 2D and Wainwright(1964)¹⁶⁾ with the equation of state by Ree&Hoover(1967)¹⁷⁾ in 3D.

The total correlation function $C(t)$ can be decomposed into pair $C_2(t)$ ($ij - ij$ collision), triplet $C_3(t)$ ($ij - ik$ collision), and quadruplet $C_4(t)$ ($ij - kl$ collision) contributions,^{11),18)} where i, j, k, l are particle index.

$$C(t) = C_2(t) + C_3(t) + C_4(t). \quad (2.5)$$

The pair contribution $C_2(t)$ is defined as,

$$C_2(t) = \frac{1}{N} \left\langle \sum_i^N \sum_{j(j>i)}^N O_{xy}^{ij}(t) O_{xy}^{ij}(0) \right\rangle = \frac{1}{2N} \frac{d^2}{dt^2} \left\langle \sum_i^N \sum_{j(j>i)}^N G^{ij}(t)^2 \right\rangle, \quad (2.6)$$

since $G^{ij}(0) = 0$ ($\dot{G}^{ij}(t) = O_{xy}^{ij}(t)$). To calculate C_2 , we introduce a “collision pair index” $c_k = (c_i - 1)N - c_i(c_i - 1)/2 + c_j - c_i$, where N is the number of particles, which identifies a given pair quickly, avoiding having to check whether the collision pair is same as before in the process of calculating $G^{ij}(t)$. This speeds up the calculation considerably. *)

§3. Results

The system consists of hard disks or hard spheres placed in a $L_x \times L_y (= A)$ square box or a $L_x \times L_y \times L_z (= V)$ cubic box, respectively, with periodic boundary conditions. Initially, the simulation systems for each packing fraction $\nu (= N\pi(\sigma/2)^2/A$

*) For example, in case of $N = 4$, the total number of collision pairs are $N(N - 1)/2 = 6$, which can be listed as $(c_i, c_j) = (1, 2), (1, 3), (1, 4), (2, 3), (2, 4), (3, 4)$, where $c_i < c_j$. By using the “collision pair index”, we obtain $c_k = 1, 2, 3, 4, 5, 6$ for each collision pair, respectively. Therefore, it is easy and convenient to deal with the collision pair as the sequential number to sort and insert the array of correlation pair $G^{ij}(t)$ when we make the computer program.

for 2D, or $(4/3)N\pi(\sigma/2)^3/V$ for 3D), are prepared as the equilibrium state by a sufficiently long preliminary run. Relative to the close packed area A_0 , and volume V_0 , $\nu = \pi/(2\sqrt{3}(A/A_0))$ and $\nu = \pi/(3\sqrt{2}(V/V_0))$, respectively. The system evolves through collisions, using an algorithm based on event-driven Molecular Dynamics (MD) simulation.¹²⁾ Most of the calculations are done with the particle number $N = 512$ and 4,096. The density is varied at relatively dense value near the solid-fluid transition point, which are known to be $\nu_c \sim 0.70$ for 2D and ~ 0.48 for 3D. Ladd & Alder (1989)¹⁰⁾ have calculated OACFs and its separate parts at several densities; $A/A_0 = 1.35, 1.4, 1.6$ for 2D and $V/V_0 = 1.5, 1.6, 1.8, 2.0$ for 3D. These densities correspond to $\nu = 0.672 \dots, 0.648 \dots, 0.567 \dots$ for 2D and $\nu = 0.493 \dots, 0.463 \dots, 0.411 \dots, 0.37 \dots$ for 3D, respectively. In our calculation, we use several additional packing fractions up to solid-fluid transition density; $\nu = 0.69, 0.67, 0.65, 0.57$ for 2D and $\nu = 0.47, 0.45, 0.40, 0.35$ for 3D.

3.1. Density & system size dependence of OACFs in 2D and 3D

First, we calculate the *total OACFs* for different packing fractions and system size to investigate the functional form of the molasses tail at long times, and the effects of periodic boundary conditions. In Figs. 1 and 2, the dimensionless OACFs for various packing fractions near the solid-fluid transition point in terms of reduced time $s = t/t_0$ for 2D and 3D are shown, respectively. Statistical averages are made over 10^{11} to 10^{12} total collisions of event-driven MD runs, which are $10^3 \sim 10^4$ larger than previous work.¹⁰⁾ Typical error bars are also shown at long times. Two different number of particles are shown in both 2D and 3D to observe periodic boundary effect due to sound wave propagation across the system. The sound wave propagation time explicitly appears in the long time tail of velocity auto-correlation functions (e.g., Ref.²⁾), but appears to have no effects here, as expected, since OACF does not involve velocities.

The OACFs for both 2D and 3D clearly show the slower decay when the system become denser and their decay are not the power law form as for the hydrodynamic tail $\sim s^{-d/2}$, where d is dimension. These data suggest that the theoretical prediction of MCT for the long time tail must be reconsidered in dense liquids. Based on these results, we choose the relatively smaller system size $N = 4096$ in 2D and $N = 512$ in 3D for efficiency to calculate C_2 in the following subsection.

3.2. Density dependence of C_2 in 2D and 3D

To investigate the density dependence of C_2 up to the time of the diffusional power regime, long runs were performed for various packing fractions. Since the maximum collision index (i.e., $c_k = N(N-1)/2$) increases as $\sim \mathcal{O}(N^2)$, it is difficult to calculate correlation functions averaged for all possible collision pairs c_k due to the restriction on CPU time and memory, if N becomes more than one thousand particles. For instance, one needs about 100Mbytes of memory for the calculation of C_2 for all possible collision pairs in the 500 particles system, comparable to the Ladd & Alder(1989) calculation, which presented no serious problem. However, in the case of $N = 4,096$ the maximum collision index becomes $c_k = 8,386,560$, which needs about 10Gbytes of main memory. To reduce the calculation to a manageable one, we

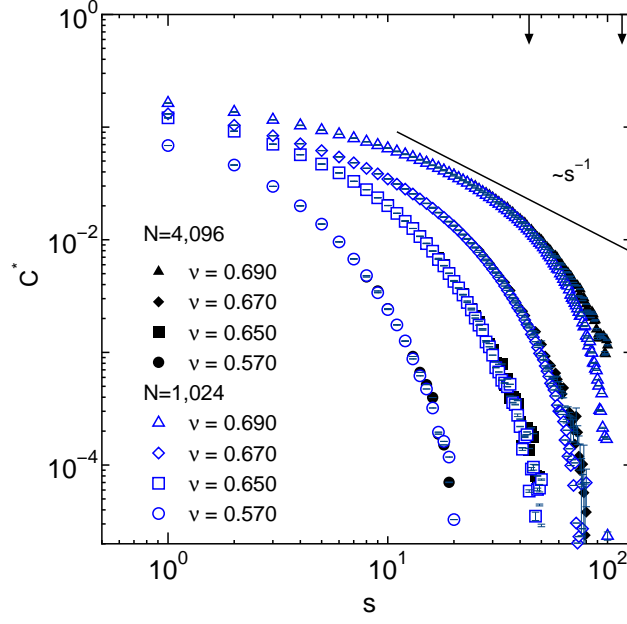


Fig. 1. A log-log plot of the dimensionless OACFs (see Eq.(2.4)) for various packing fractions for two different sized systems in 2D versus reduced time, $s = t/t_0$ are shown. Arrows describe the approximate values of the sound wave transversal time (the left for $N = 1024$ and the right for $N = 4096$.)

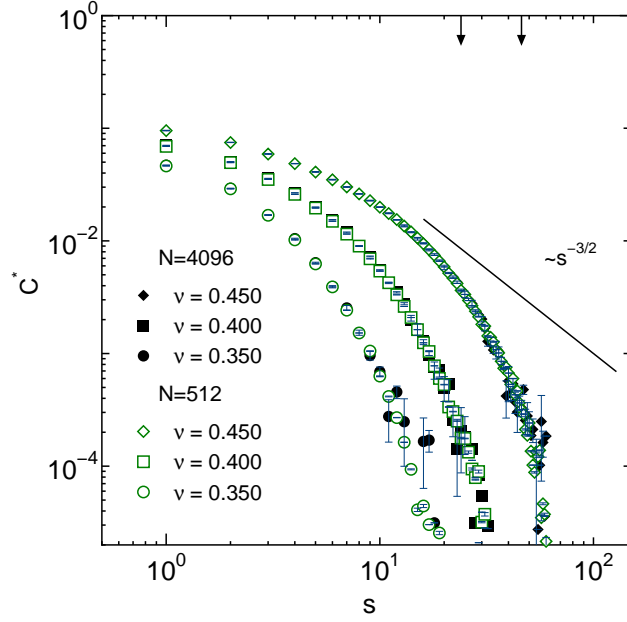


Fig. 2. As Fig.1 except for 3D.

restrict the range of collision pairs c_k from 1 to $10N$ in the averaging procedure. This restriction of c_k only affects to error bars, but we perform sufficiently long time MD runs for C_2 , much longer than the typical time scale of the largest cluster breaking up.

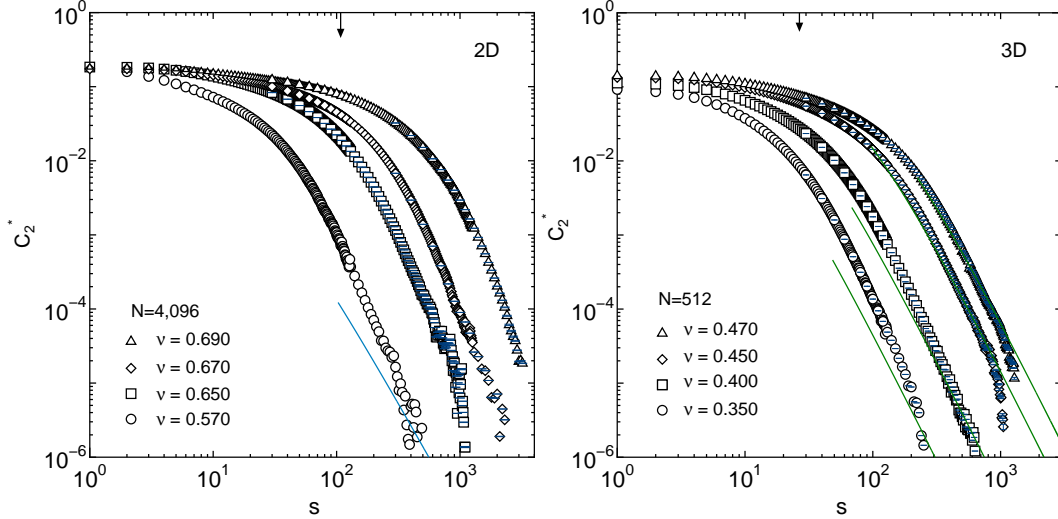


Fig. 3. C_2^* s for various packing fractions near the solid-fluid transition point in 2D (left) and 3D (right) in terms of reduced time $s = t/t_0$. Arrows indicate the sound wave transversal time for each system size. Theoretical slopes by using the effective diffusion constant at $\nu = 0.57$ in 2D(left) and the diffusion constant obtained from actual simulation for each packing fraction in 3D(right) at long times are given by the lines (see, Sec. 3.4).

We performed up to 10^{12} collision for several independent runs for different time resolution, namely $\Delta t = t_0, 10t_0$, and $100t_0$ at each packing fraction. We confirmed that these runs give consistent results. The efficiency of these calculation is such that it does not significantly slow down the MD calculation. The error bars in the figures are smaller than the symbols except at a few points at long times. As indicated in Fig. 3, C_2 in both 2D and 3D decays slower as the density becomes higher. The results are consistent with both our previous method at $\nu = 0.65$ ¹¹⁾ and Ladd & Alder(1989).¹⁰⁾ It is interesting to observe that qualitatively the decay is similar for 2D and 3D. Next, we investigate the decay of C_2 in the two separate time regime, namely the molasses and diffusional regimes.

3.3. Molasses regime in C_2

We investigate the scaling behavior in the molasses regime as we did previously.¹⁰⁾ In the molasses regime, C_2^* was found to have a scaling law of the stretched exponential form as,

$$C_2^*(t) = B \exp \left[- \left(\frac{t}{t_2} \right)^\alpha \right], \quad (3.1)$$

where t_2 is the relaxing time in the molasses regime and α is a density “independent” stretched exponent. The value of the exponent α was found to be ~ 0.80 for 2D

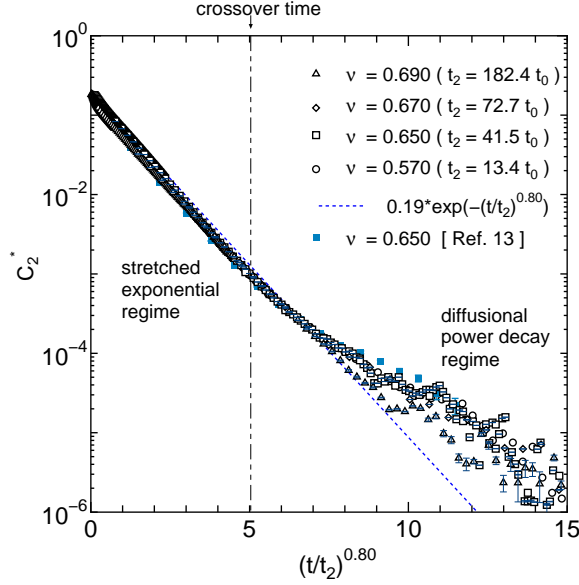


Fig. 4. Decay of the C_2^* in a semilog plot for 4096 particles against the scaled time $(t/t_2)^{0.8}$ for the several packing fractions in 2D.

and ~ 0.70 for 3D in previous work.¹⁰⁾ By adopting a simple fitting method to C_2 as given by eq. (3.1) with the given values of α , we estimated t_2 . C_2^* for the several packing fractions plotted against the scaled time $(t/t_2)^\alpha$ are shown in Figs. 4 and 5. We found that the curves for various packing fraction collapse to a straight line in the regime of $(t/t_2)^\alpha$ between 1 and 5. Thus, the decay of C_2^* is in good agreement with the stretched exponential form of eq. (3.1), which is a similar result given in Ref.¹⁰⁾ The crossover time t_{cs} from the molasses regime to the diffusional power regime in terms of the mean free time t_0 are summarized in Table I and Fig. 6.

packing fraction(2D)	ν	0.57	0.65	0.67	0.69
crossover time	t_{cs}/t_0	100	287	536	1364
packing fraction(3D)	ν	0.35	0.40	0.45	0.47
crossover time	t_{cs}/t_0	55	115	281	431

Table I. The crossover time t_{cs} from stretched exponential to power form in terms of the mean free time t_0 for various packing fractions are shown.

The log of the crossover time is increasing linearly in 3D, but faster than exponential in 2D with packing fraction near the solid-fluid transition point ν_c .

3.4. Diffusional regime in C_2

In the regime of $(t/t_2)^\alpha > 6$, the data show a different functional form from the molasses regime, in which the correlation function changes from a stretched exponential to a power decay,

$$C_2^*(t) = B't^{-\beta}, \quad (3.2)$$

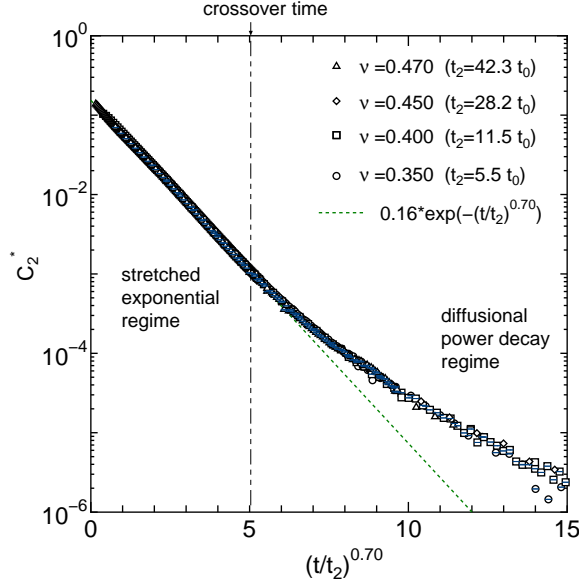


Fig. 5. Decay of the C_2^* in a semilog plot for 512 particles against the scaled time $(t/t_2)^{0.7}$ for the several packing fractions in 3D.

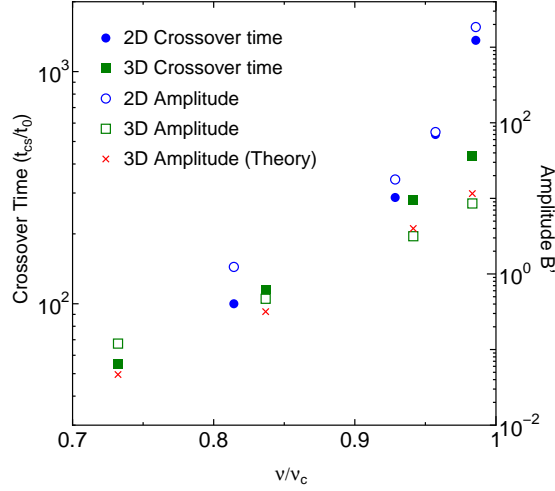


Fig. 6. The log of the crossover time t_{cs} divided by the mean free time t_0 and the log of the amplitude B' , both as a function of the packing fraction given relative to the freezing point.

where β and B' are the exponent and the amplitude, respectively. From past theoretical work based on MCT and the pair diffusion mechanism, it is predicted that $\beta = 7/2$ in 3D. Leegwater&Beijeren(1989)¹⁹⁾ investigated the equation for two particles diffusing relative to each other, which predicts at long times the behavior of C_2 as

$$C_2^*(t) = \frac{2\pi n t_E}{15\beta\eta_E} (n\sigma^3 g(\sigma)) \left(\frac{\sigma^2}{4Dt} \right) \exp\left(-\frac{\sigma^2}{4Dt}\right) I_{5/2}\left(\frac{\sigma^2}{4Dt}\right) \quad (3.3)$$

$$\simeq \frac{2\sqrt{2\pi} n^2 t_E \sigma^3 g(\sigma)}{225\beta\eta_E} \left(\frac{\sigma^2}{4D} \right)^{\frac{7}{2}} t^{-\frac{7}{2}} \quad (t \rightarrow \infty), \quad (3.4)$$

where $n = N/V$ is the number density, D is diffusion constant, E stand for Enskog, $g(\sigma)$ is the pair distribution function at contact, and $I_{5/2}$ is a modified Bessel function. They also found that a modified theoretical prediction by incorporating recollision contribution and a potential of mean force is in excellent agreement with the MD data throughout the intermediate-time and long-time regimes $t/t_0 > 10$, although this requires an effective diffusion constant about 10% less than for a single particle.¹⁹⁾ By the same theoretical argument applied to the 2D,²⁰⁾ we obtain

$$C_2^*(t) = \frac{\pi n t_E}{8\beta\eta_E} (n\sigma^4 g(\sigma)) \left(\frac{\sigma^2}{4Dt} \right) \exp\left(-\frac{\sigma^2}{4Dt}\right) I_2\left(\frac{\sigma^2}{4Dt}\right) \quad (3.5)$$

$$\simeq \frac{\pi n^2 t_E \sigma^4 g(\sigma)}{64\beta\eta_E} \left(\frac{\sigma^2}{4D} \right)^3 t^{-3} \quad (t \rightarrow \infty), \quad (3.6)$$

In 2D, the theoretical decay is $C_2(t) \sim t^{-3}$ in the long time limit.

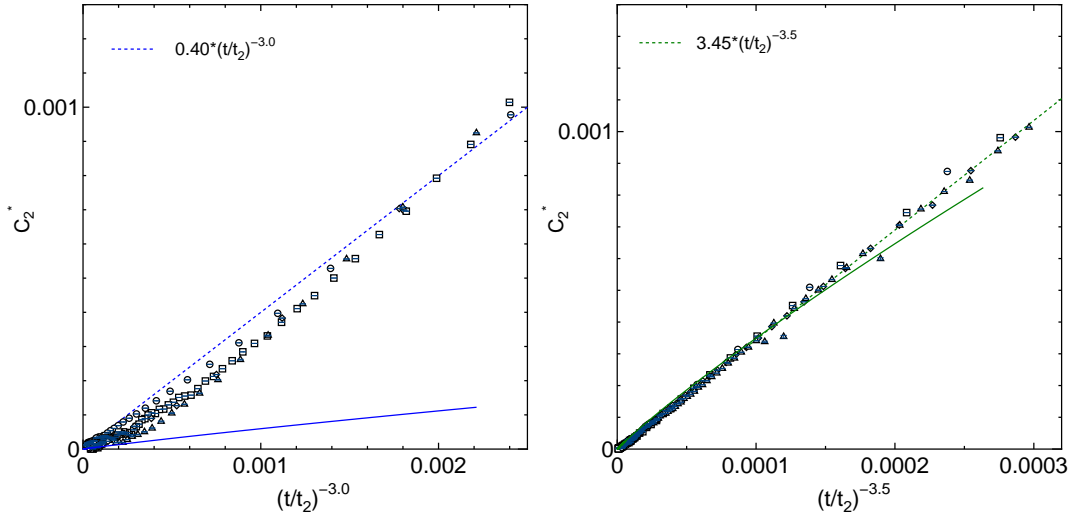


Fig. 7. Decay of C_2^* in the diffusional power decay regime in terms of $(t/t_2)^{-\beta}$ for the several packing fractions in 2D(left) and 3D(right) for 4096 and 512 particles are shown. The solid lines are theoretical results for $\nu = 0.57$ in 2D(left) and $\nu = 0.47$ in 3D(right), respectively. The dot lines are the linear fitting lines.

Plotting C_2^* in terms of $(t/t_2)^{-7/2}$ in Fig. 7, in the 3D case the data lead to a linear function, which indicates consistency only with the exponent of theoretical prediction of $\beta = 7/2$ in the long time limit. In the 2D case, numerical data suggest the exponent

deviates from $\beta = 3$. Because of the divergence of the diffusion coefficient in 2D, the entire theory needs to be reworked. The amplitudes of the simulation data in 3D are in fairly good agreement with the theoretical results incorporating recollision contributions and a potential of mean force through the extra factor of $g(\sigma)$, (i.e., $(25/9)g(\sigma)C_2^*(t)$ in the long time limit), as shown in Fig. 3, 6 and 7, which are described in Ref.¹⁹⁾ In Table II, the values of amplitude B' of eq. (3.2) are shown. We also show B' in terms of scaled packing fraction (ν/ν_c : ν_c is solid-fluid transition point) in Fig. 6.

packing fraction(2D)	ν	0.57	0.65	0.67	0.69
Amplitude	B'	1.42	17.8	75.5	1849
packing fraction(3D)	ν	0.35	0.40	0.45	0.47
Amplitude	B'	0.12	0.47	3.16	8.57
Amplitude(Theory)	B'	0.047	0.32	4.00	11.58

Table II. The amplitude B' for various packing fractions are given and plotted in Fig. 6.

§4. Discussion

The cause of the stretched exponential relaxation in the molasses regime is considered to be due to the distribution of different life times of transient clusters of nuclei in dense fluid systems. Thus, there exist several exponential relaxation decays for each collision pair. To confirm the above speculation for the origin of the molasses effect in 2D at the microscopic level, we calculated the bond orientational order, ϕ_6 as an alternative to C_2 , and furthermore, to visualize the distribution of crystal clusters in the hard disk system. The usual bond orientational order parameter ϕ_6 for each hard disk i is defined by

$$\phi_6^i = \left| \frac{1}{N_i} \sum_{j=1}^{N_i} \exp(6i\theta_{ij}) \right|, \quad (4.1)$$

where N_i is the number of the nearest neighbors around the tagged particles i , and θ_{ij} is the angle between the position vector from the disk j to i and an arbitrary fixed reference axis (e.g., x -axis). Two disks are defined as neighbors if the distance is less than $\sqrt{3}\sigma$. In this definition, ϕ_6^i takes on values between 0 and 1, which measures the degree of crystallization in terms of considering only nearest neighbors.

Figure 8 shows typical snapshots of the spatial distribution of ϕ_6^i . The gradation in shading of the particles indicate the value of ϕ_6^i , the darker, the closer to unity. We clearly observe the dramatic growth of several solid nuclei as the density nears solidification. The averaged values of ϕ_6^i and the number of particle with $0.9 < \phi_6^i < 1$ for each packing fraction are summarized in Table III.

Understanding the slow decaying process of the OACF is considered a key factor in understanding the onset of the glass transition, and is here qualitatively confirmed to be due to the transitory existence of solid nuclei in 2D in Fig. 8. Recently, their existence was also demonstrated in colloid experiments.²¹⁾ For quantitative purposes

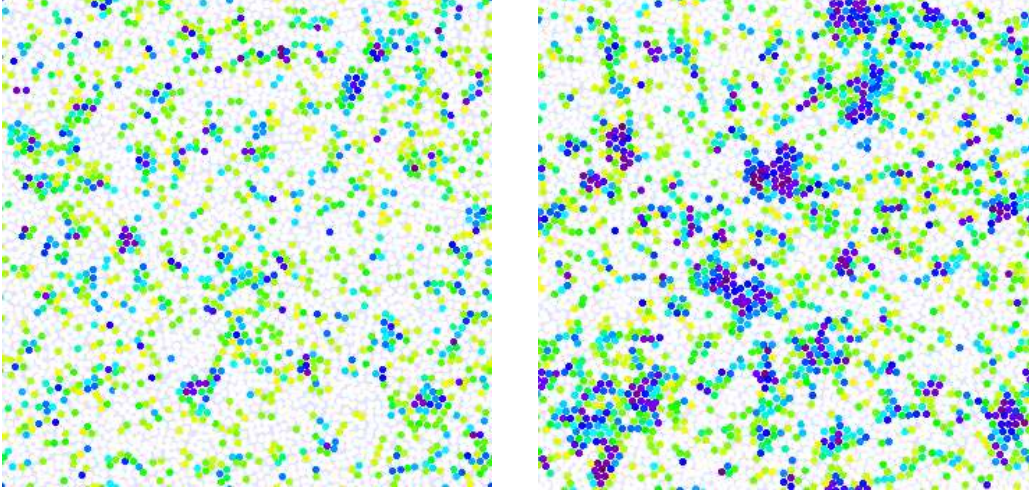


Fig. 8. The spatial distribution of ϕ_6^i for 4096 particles system at a given time for two packing fractions, $\nu = 0.65$ (left) and 0.69 (right). The darker the region, the closer ϕ_6 is to unity.

packing fraction(2D)	ν	0.57	0.65	0.67	0.69
averaged bond orientational order	$\overline{\phi_6^i}$	0.36	0.42	0.44	0.47
particle number with $0.9 < \phi_6^i < 1$	N_s	11	58	82	131

Table III. The averaged bond orientational order $\overline{\phi_6^i}$ and the number of particle with $0.9 < \phi_6^i < 1$ for various packing fractions are shown.

it is crucial to determine the spatial extents of the crystal nuclei and how long they persist. In that direction we quantitatively determined in this paper that the decay of the pair distribution of C_2 could be characterized by a relaxation time t_2 at intermediate time (molasses regime) and later on by a pair diffusional breaking up of the clusters. At the quantitative crossover time shown explicitly in Table I and Fig.6, the largest cluster at the freezing density of only a few sphere diameter in size persist for $\sim 431t_0$, which corresponds for typical argon parameters estimate of $t_0 \sim 6.4 \times 10^{-14}$ [s] to only about 30 picoseconds ($\sim 2.8 \times 10^{-11}$ [s]) in real liquids. To make the further quantitative progress, we need to investigate the orientation correlation function of the quadruplet component, C_4 , as a function of the distance between the two colliding pairs. When this is carried out as a function of density, it could be possible to tell how the cluster size distribution changes and how long they last as the solidification density is approached, and, subsequently, determine how fast one has to increase the density to get a glass instead of a crystal. This is however, computationally a very demanding task. Instead we are planing to investigate an extension of ϕ_6^i to a higher order orientational parameter involving further neighbors and thus, hopefully, improve the methodology of an alternative efficient calculation for $C_4(t)$.

Acknowledgements

We would like to thank Professor A.J.C. Ladd for helpful comments. We also wish to thank Professors H. Mori, H. van Beijeren, W.G. Hoover, D. Frenkel, N. Ito and J. Wakou for valuable discussions. This study was supported by Grant-in-Aid for Scientific Research from the Ministry of Education, Culture, Sports, Science and Technology No. 19740236. Part of the computations for this study was performed using the facilities of the Supercomputer Center, Institute for Solid State Physics, the University of Tokyo, and Research Center for Computational Science, Okazaki, Japan.

References

- 1) B. J. Alder and T. E. Wainwright, Phys. Rev. Lett. **18** (1967), 988; J. Phys. Soc. Jpn. Suppl. **26** (1969), 267; Phys. Rev. A **1** (1970), 18.
- 2) M. Isobe, Phys. Rev. E **77** (2008), 021201; Prog. Theor. Phys. Suppl. No. 178 (2009), 72.
- 3) B. J. Alder, in *Molecular Dynamics Simulation of Statistical-mechanical Systems*, edited by G. Ciccotti and W. G. Hoover, (North-Holland, Amsterdam, 1986) p. 66.
- 4) J. R. Dorfman and T. R. Kirkpatrick, in *Molecular Dynamics Simulation of Statistical-mechanical Systems*, edited by G. Ciccotti and W. G. Hoover, (North-Holland, Amsterdam, 1986) p. 260.
- 5) D. J. Evans, J. Stat. Phys. **22** (1980), 81.
- 6) W. W. Wood and J. J. Erpenbeck, J. Stat. Phys. **24** (1981), 455.
- 7) G. P. Morriss and D. J. Evans, Phys. Rev. A **32** (1985), 2425.
- 8) W. Götze and L. Sjögren, Rep. Prog. Phys. **55** (1992), 241.
- 9) W. Götze, *Complex Dynamics of Glass-Forming Liquids* (Oxford Univ. Press, Oxford, 2008).
- 10) A. J. C. Ladd and B. J. Alder, J. Stat. Phys. **57** (1989), 473.
- 11) M. Isobe and B. J. Alder, Mol. Phys. **107** (2009), 609.
- 12) M. Isobe, Int. J. Mod. Phys. C **10** (1999), 1281.
- 13) E. Helfand, Phys. Rev. **119** (1960), 1.
- 14) B. J. Alder, D. M. Gass and T. E. Wainwright, J. Chem. Phys. **53** (1970), 3813.
- 15) D. M. Gass, J. Chem. Phys. **54** (1971), 1898.
- 16) T. E. Wainwright, J. Chem. Phys. **40** (1964), 2932.
- 17) F. H. Ree and W. G. Hoover, J. Chem. Phys. **46** (1967), 4181.
- 18) A. J. C. Ladd, T. A. Litovitz and C. J. Montrose, J. Chem. Phys. **71** (1979), 4242.
- 19) J. A. Leegwater and H. van Beijeren, J. Stat. Phys. **57** (1989), 383.
- 20) J. Wakou, private communication (2010).
- 21) J. C. Conrad, P. P. Dhillon, E. R. Weeks, D. R. Reichman and D. A. Weitz, Phys. Rev. Lett. **97** (2006), 265701.